

14th CIRP Conference on Modeling of Machining Operations (CIRP CMMO)

Modeling Static and Dynamic Cutting Forces and Vibrations for Inserted Ceramic Milling Tools

I. G. Euan^{ac}, E. Ozturk^{b*}, N. D. Sims^c

^a Centro de Ingenieria y Desarrollo Industrial, Pie de la Cuesta 702, 76130 Queretaro, Qro., Mexico

^b AMRC with Boeing, The University of Sheffield, Advanced Manufacturing Park, Wallis Way, Catcliffe, Rotherham, S60 5TZ, UK

^c Department of Mechanical Engineering, The University of Sheffield, Sir Frederick Mappin Bldg, Mappin St, Sheffield, S1 3JD, UK

* Corresponding author. Tel.: (+44) (0) 114 222 66 71; fax: (+44) (0) 114 222 76 78. E-mail address: e.ozturk@amrc.co.uk

Abstract

Cutting tools with ceramic inserts are increasingly being used in machining of super alloys typically used in aerospace industry. The ceramic inserts make higher cutting speeds possible due to the higher temperature resistance compared to carbide inserts. However, the success of the process is very sensitive to the right selection of process parameters. In this study, analytical process models for indexable milling tools with round ceramic inserts are presented. These models can be used to determine the cutting parameters for optimum quality and maximum productivity. Firstly, geometry of the insert cutting edges under the effect of angles on the inserts was formulated. Then, an analytical cutting force model was developed. This allows analyzing the effects of the parameters on the cutting forces. A time-domain model was also developed to analyze the dynamic cutting forces and stability limits for the milling process. Afterwards, the models were implemented in a Matlab® GUI to make the applications of the models in the industry easy. Cutting force coefficients, which are needed to calculate cutting forces, were identified from cutting tests with Inconel 718 material. Then, the cutting force model was validated with cutting experiments. After obtaining modal data of the tool via tap testing, dynamic cutting forces and vibrations were simulated by means of the time domain model. A series of simulations was carried out to determine stability limits at certain operating conditions using the time domain model, and stability lobes for the tools under study were plotted.

© 2013 The Authors. Published by Elsevier B.V. Open access under [CC BY-NC-ND license](https://creativecommons.org/licenses/by-nc-nd/4.0/).

Selection and peer-review under responsibility of The International Scientific Committee of the “14th CIRP Conference on Modeling of Machining Operations” in the person of the Conference Chair Prof. Luca Settineri

Keywords: *indexable tool, cutting forces, ceramic inserts, vibrations*

1. Introduction

Round ceramic inserts represent economic advantages over other type of inserts since higher material removal rate (MRR) is possible owing their high heat resistance and gradual entry to the cut. Analytical process models, that allow reliable predictions of cutting forces and machine-tool vibrations, facilitate the optimum process parameter selection, which is a challenge before making cutting tests. Main concerns are to control the cutting forces and to avoid chatter vibrations, as high and fluctuating cutting force magnitudes generally indicate chatter. This is the major limiting factor for increasing MRR, as it may cause severe machining problems [1]. Besides, power consumption and tool life are dependent on cutting force magnitudes.

Several researchers have been working in analytical, numerical and experimental models for predicting

cutting forces and vibrations. In the past, the research was focused on modeling the mechanics and dynamics of standard end and face milling cutters with different geometries, such as cylindrical, ball-end and tapered. Indexable tools appeared in the mid-20th century. Fu et al. [2] presented pioneering work in the study of inserted face milling cutters. Engin and Altintas [3] developed a generalized mathematical model for inserted cutters, but it was experimentally validated for rectangular shapes. Recently, Altintas et al. [4] presented a unified cutting force model for inserted cutters that can be applied for different types of machining operations, but it is experimentally verified for straight line cutting edges too. Kim et al. [5] and Liu et al. [6] considered round cutting edges in the cutting force calculations which were experimentally verified, but the dynamic part of the forces was not taken into account.

In the next section, geometry of the cutting edge on the insert is described. In section 3, the cutting force model is detailed. The time-domain model is explained in section 4. In section 5, the verification of the static and dynamic forces with experimental data is exposed. Finally, stability analysis and conclusion are presented in section 6 and 7 respectively.

2. Tool geometry

The tool of interest is shown in Fig. 1; its geometric model is developed based on the work presented by Engin and Altintas [3].

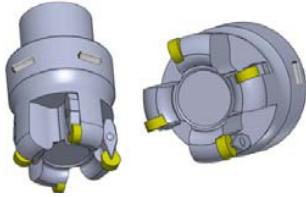


Fig. 1. Indexable tool with round inserts.

Fig. 2 presents the insert geometry. The cutter body is aligned with the global Cartesian coordinate system (X, Y, Z) and the insert with a local Cartesian coordinate system (u, v, w) . The angular offset (φ) is measured counter clockwise from the Y axis, I_r is the radial offset in the XY plane and I_z is the axial offset of the insert center (O') from the XY plane.

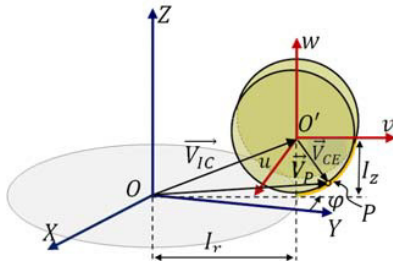


Fig. 2. Insert geometry.

The round insert is defined by the radius (R_i) , (Fig. 3). During milling the insert edge has two angular boundaries (θ_s, θ_e) that define the cutting edge. The vector V_{CE} defines locally the cutting edge of the insert.

$$\vec{V}_{CE} = u\vec{i} + v\vec{j} + w\vec{k} \quad (1)$$

$$u = 0; \quad v = R_i \cos \theta; \quad w = -R_i \sin \theta; \quad \theta_s \leq \theta \leq \theta_e$$

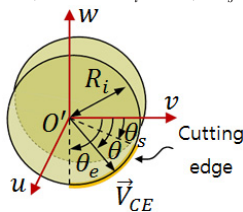


Fig. 3. Geometry of a round insert.

The insert is rotated around the local axes (u, v, w) to orientate it in the cutter body, using the global coordinate system (X, Y, Z) as reference. Fig. 4 shows the initial position of the insert and the rotations that define the final orientation. As the insert is round, only the rotation around v and w axis are important from a modeling point of view.

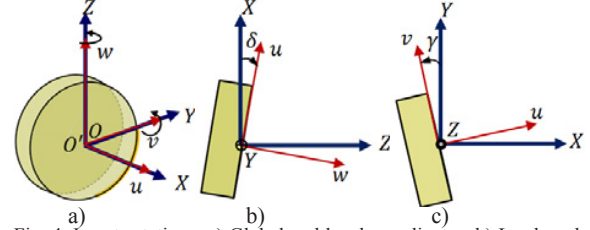


Fig. 4. Insert rotations. a) Global and local coordinates. b) Lead angle. c) Index angle.

Firstly, the insert is rotated the lead angle δ about Y and after about Z axis with index angle γ . The resulting transformation matrix is:

$$T_{M1} = \begin{bmatrix} \cos \delta \cos \gamma & -\sin \gamma & \cos \gamma \sin \delta \\ \cos \delta \sin \gamma & \cos \gamma & \sin \delta \sin \gamma \\ -\sin \delta & 0 & \cos \delta \end{bmatrix} \quad (2)$$

After rotations, the coordinates of the cutting edge in the insert coordinate system are described by the vector \vec{V}_{CER} .

$$\vec{V}_{CER} = T_{M1} \cdot \vec{V}_{CE} \quad (3)$$

Finally, the insert is placed in the cutter body. The position of the cutting edge with respect to the cutting body is given by the vector (\vec{V}_P) .

$$\vec{V}_P = \vec{V}_{IC} + \vec{V}_{CER} \quad (4)$$

Hence, once the center location (I_r, I_z) , edge dimensions (R, θ_s, θ_e) and orientation (δ, γ) are defined, any point (P) in the edge can be evaluated using Equation 4. It is defined globally by the vector \vec{V}_P and locally by the vector \vec{V}_{CER} .

3. Cutting force model

The insert cutting edge is discretized in several points and the cutting force components are calculated at each of these points whenever they are located in the cut region. Calculation of tangential (dF_t) , radial (dF_r) and axial (dF_a) differential forces is given by:

$$dF_t = K_{te} dS + K_{tc} h(\phi, \kappa) db$$

$$dF_r = K_{re} dS + K_{rc} h(\phi, \kappa) db \quad (5)$$

$$dF_a = K_{ae} dS + K_{ac} h(\phi, \kappa) db$$

The equations are expressed as a function of the instantaneous chip thickness $h(\phi, z)$, the width of chip (db) , the curved edge contact length (dS) , and the cutting force coefficients: $K_{te}, K_{re}, K_{ae}, K_{tc}, K_{rc}$ and K_{ac} (Fig. 5) [7].

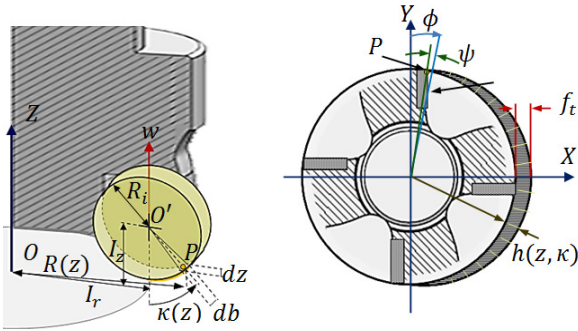


Fig.5. Process parameters and geometry involved in the cutting force calculation.

The chip thickness is measured normal to the cutting edge, and it is defined in Equation 6. Where f_t , ϕ and κ (Fig. 5) denote the feed per tooth, the radial immersion angle and the axial immersion angle, respectively.

$$h(\phi, \kappa) = f_t \sin \phi \sin \kappa \tag{6}$$

Equations to calculate db , κ , ϕ and the radial immersion angle (ψ), are analogous to the arc zone of a general end mill [8]. Therefore they are not repeated here. As the discretization of the insert in the axial direction is relatively small, dS is assumed to be equal to db .

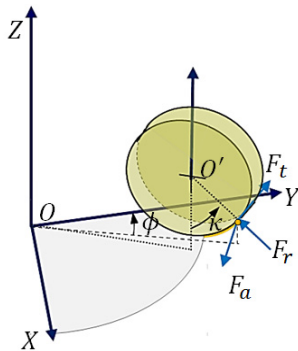


Fig. 6. Cutting force directions.

Fig. 6 shows the cutting force directions at one point of the cutting edge of the j -th insert. The transformation of the differential cutting forces in feed (X), normal (Y) and axial (Z) directions into tangential (dF_t), radial (dF_r) and axial (dF_a) differential cutting forces at each point of the cutting edge, is given by:

$$\begin{bmatrix} dF_x \\ dF_y \\ dF_z \end{bmatrix} = \begin{bmatrix} -\cos\phi & -\sin\kappa\sin\phi & -\cos\kappa\sin\phi \\ \sin\phi & -\sin\kappa\cos\phi & -\cos\kappa\cos\phi \\ 0 & \cos\kappa & -\sin\kappa \end{bmatrix} \begin{bmatrix} dF_t \\ dF_r \\ dF_a \end{bmatrix} \tag{7}$$

The cutting forces of the j -th insert in the principal directions at each radial immersion angle are obtained by integrating the cutting forces along and the axial depth of cut, defined by the boundaries z_1 and z_2 , within the engagement boundary. Finally, the contribution of N

inserts should be summed to calculate the total cutting forces at each direction.

$$F_{qj}(\phi_j) = \sum_{j=1}^N \int_{z_1}^{z_2} dF_{qj}(\phi_j, z); q = x, y, z \tag{8}$$

3.1. Cutting force coefficients (CFCs)

CFCs depend on the tool and work piece interaction, which is controlled by the cutting parameters. CFC calculation is performed with the semi-empirical mechanistic method outlined by Altintas and Budak [1] for cylindrical end mills. This technique requires sets of milling tests at different feeds per tooth and cutting speeds. In each set, it is required to average the cutting forces for each direction at several feeds per tooth (f_t) but at the same cutting speed (sp). Linear dependency of the average forces with respect to the feed rate is assumed. Analytical expression for the average cutting forces is presented in the equation below [8]:

$$\bar{F}_{xyz} = \frac{1}{\phi_p} \int_{\phi_{st}}^{\phi_{ex}} \int_{z_1}^{z_2} dF_{xyz}(\phi, z) d\phi \tag{9}$$

Where $\phi_n = 2\pi/N$ is the pitch angle for a cutter with N uniformly space inserts, ϕ_{st} and ϕ_{ex} are the start and exit radial immersion angles, and z_1 and z_2 are the axial cut boundaries.

3.2. Engagement boundaries

Engagement angles, start angle ϕ_{st} and exit angle ϕ_{ex} , define the engagement boundaries of the cutting zone. Cutting forces on an insert occur only when the insert cutting edge of the tool is within these boundaries: $dF_x(\phi), dF_y(\phi), dF_z(\phi) > 0$ when $\phi_{st} \leq \phi \leq \phi_{ex}$ (10)

Where ϕ is the local radial immersion angle. Engagement angles depend on the type of milling operation and the geometry of the tool. In slot milling, the engagement angles are $\phi_{st} = 0^\circ$ and $\phi_{ex} = 180^\circ$. Up milling and down milling geometries are shown in the following figure.

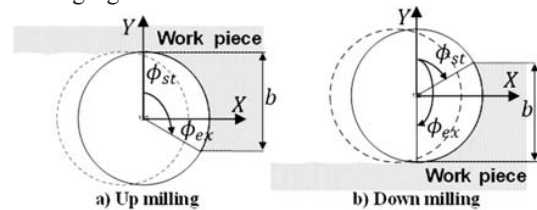


Fig. 7. Geometry of milling process.

The radius of the tool is variable along the tool axis due to the insert radius. Therefore, the local radius is used instead of the tool radius in engagement boundary calculations, Hence the engagement boundaries are

location dependent along the tool axis. Engagement angles are calculated based on Ozturk et al.'s work [9].

4. Time-domain model

The time-domain model was developed based on the regenerative force, dynamic deflection model by Smith and Tlustý [10]. The tool is modeled as a non-rigid body to consider its deflections. During the milling process the dynamic cutting forces excite the structural modes of the machine-tool-work piece system and a wavy surface is left in each tooth period, which is removed by the subsequent oscillatory tooth. Hence, the dynamic chip thickness may become oscillatory and grow exponentially depending on the phase shift of the waves. Consequently higher displacements of the tool tip and higher cutting forces at the progressive cycles result. The time domain model is capable of predicting this behavior by simulating the dynamic chip thickness, the forces and the displacements at discrete time steps.

4.1. Dynamic chip thickness

Dynamic chip thickness depends on the feed per tooth, present and previous tooth period vibrations. The milling tool is considered to have two orthogonal degrees of freedom. Dynamic displacements in X (feed) and Y (normal) directions are calculated when the cutting forces excite the structure in these directions. Dynamic displacement at a given instant is written as follows:

$$v_j = -x \cdot \sin \phi_j - y \cdot \cos \phi_j \quad (11)$$

Where x , y are the displacement component magnitudes in feed and normal directions, respectively. The instantaneous angular immersion ϕ_j is a function of time, $\phi_j = sp \cdot t$; where sp is the spindle speed in rpm. Then, the equation for dynamic chip thickness is written as:

$$h(t) = f_t \cdot \sin \phi_j \cdot \sin \kappa + v_{j,0}(t - \tau) - v_j(t) \quad (12)$$

Where the tooth period (τ) is defined as $\tau = 60/(sp \cdot N)$; and $v_j, v_{j,0}$ are the dynamic displacements of the cutting tool at the present and previous tooth periods, respectively.

4.2. Dynamic displacements

To calculate the dynamic displacement, the tool is considered as a system consisting of single degree of freedom masses in X and Y directions. The motion in X and Y direction is described by:

$$\begin{aligned} m_x \ddot{x} + c_x \dot{x} + k_x x &= F_x \\ m_y \ddot{y} + c_y \dot{y} + k_y y &= F_y \end{aligned} \quad (13)$$

Expressions for the accelerations in X and Y directions in the current time step are derived from the equation of motion. The present acceleration is calculated using the velocities and the positions from the previous time step. The initial velocities and positions are equal to zero for the first step time. The present positions are determined by numerical integration using Euler method. The dynamic cutting forces are determined using the Equation 5, but considering the dynamic chip thickness instead of the static chip thickness.

4.3. Measurements of the FRFs

Direct tool tip frequency response functions, FRF_{xx} and FRF_{yy} , were measured through a static tap test (Fig. 8) in order to obtain modal parameters (natural frequency, damping and stiffness for each mode), necessary to characterize the non-rigid behavior of the tool in X and Y directions in the time domain model.

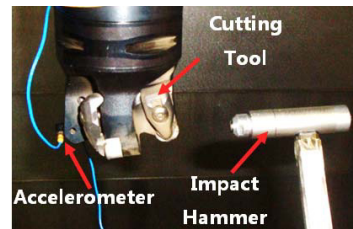


Fig. 8. Tap testing set up.

5. Verification of the force models

The force model was verified through a cutting force experiment. Two indexable tools were used. The first one has 4 negative round ceramic inserts and the other one has 5 positive round ceramic inserts. Both tools are 63 mm of diameter and all inserts are 12.7 mm in diameter. First tool has an axial rake angle of -7° and a radial rake angle of -13° . Second tool has 0 axial rake angle and radial rake angle of -3° . A StarragHeckert ZT-1000 machine was used to perform the cuts. The work piece material was Inconel 718. The process was slot milling and the axial depth was 1.5 mm. The cutting tests were done at 4353, 4761 and 5169 rpm with each type of tool. The feed rate was varied at each of these spindle speeds. The feed rates values were 0.0465, 0.0775, 0.0969, and 0.1162 mm/tooth. Then, 12 tests were done for each cutting tool. The cutting forces were measured using a Kistler 9255B dynamometer. Fig. 9 shows the force measurement set-up.



Fig. 9. Measurement of the cutting forces.

CFCs were estimated using a Matlab® algorithm which was implemented in a graphical user interface (GUI). As an example, Table 1 presents the calculated CFCs at the rotational speed of 5169 rpm (cutting speed of 875 m/min). For large negative rake angles, K_{rc} can be considerably higher than K_{ic} , as seen for the first tool.

Static and dynamic cutting force models were also integrated to the GUI. Then the cutting forces were predicted and compared with the experimental data. As run-out effect was clearly observed in the measured cutting forces in some of the tests, it was integrated to the static force model in order to have a better agreement with the experimental cutting forces. This was done by distributing the feed rate unevenly among the inserts.

Table 1. Calculated CFCs.

Tool	K_{ic} MPa	K_{rc} MPa	K_{ac} MPa	K_{te} N/mm	K_{re} N/mm	K_{ae} N/mm
1st	3700.4	20656.4	-1769.7	30.1	111.2	12.7
2nd	2665.5	2134.6	-377.5	29.3	285.2	22.05

A representative case of the cutting force comparison for each tool type is shown in Fig. 10 for one tool revolution. In Fig. 10 (b) the run-out effect, which caused uneven force contributions among the teeth, is clearly observed in the measured cutting forces. However, run-out effect was not observed in the force measurement for Tool 1 presented in Fig 10(a), therefore this effect was not considered for simulations with this tool. In the simulation for Tool 2, the run-out effect was considered in the static force model. Hence the static force model is able to predict the uneven force distribution among the teeth. This effect was not included in the dynamic force model, thus there is a slight discrepancy between the static and dynamic cutting force predictions on some teeth. Otherwise, they both would give the same predictions as it is the case in Fig. 10(a).

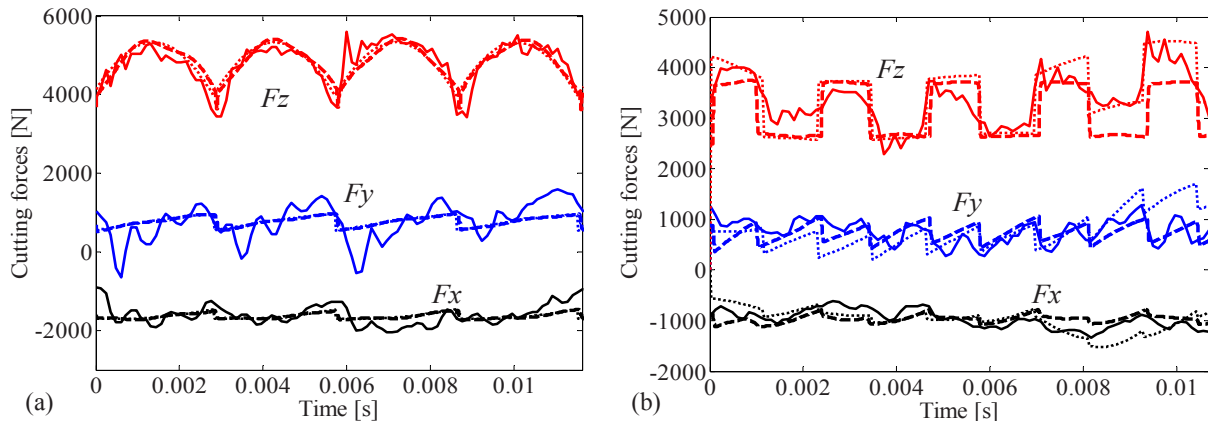


Fig. 10. Comparison of measured cutting forces (solid line), simulated static cutting forces (dotted line) and simulated dynamic cutting forces (dashed line), 100% radial immersion, $sp=519$ rpm, $f_t=0.116$ mm/tooth. a) First tool. b) Second tool.

According to simulations, experimental cutting tests were done under stable conditions since the dynamic part of the chip thickness is not significant. Therefore simulated dynamic cutting forces are very close to the simulated cutting forces using the rigid tool model. The cutting forces of the first tool are 45 % greater in F_x , 35% in F_y and 75% in F_z approximately, with respect to the second tool (Fig. 10) this is cause by the different insert orientation angles. Cutting force variations are more evident for the second tool force comparison. However, for both cases, there is a good agreement between the measured and predicted forces.

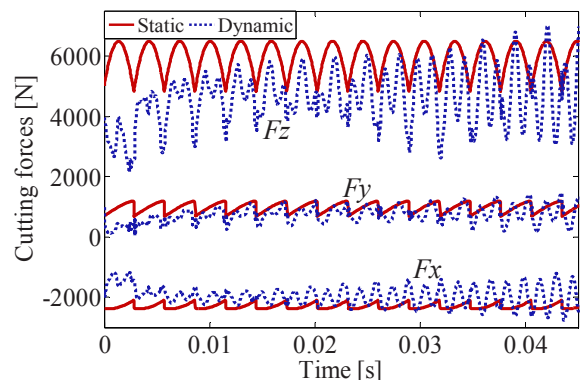


Fig. 11. Cutting force comparison under unstable conditions. First tool, slot milling, $sp = 5169$ rpm, $f_t = 0.116$ mm/tooth, $a = 2$ mm.

The small force fluctuations seen in the experimental data can be due to excitation of the dynamometer in its natural frequencies. Unlike flat-end mills the axial force (F_z) is the biggest force magnitude for the tool type under analysis, due to the insert radius. An example of cutting forces under unstable conditions is presented in Fig. 11, where static cutting forces remain stable meanwhile dynamic cutting forces increasing their magnitude over time (unstable effect).

6. Stability analysis

Using the time-domain model, some operating conditions were set to find the stability limits and sketch the stability lobes. The estimated maximum axial depth of cut that ensure a stable milling process for the experimental spindle speeds are tabulated in Table 2. CFCs for the spindle speeds under analysis were averaged to estimate the stability lobes (Fig. 12 and Fig. 13). The second tool has higher stability limits and lower cutting forces than the first tool. This could be associated with the lower force magnitudes in the second tool as shown in Fig. 10.

Table 2. Stability limits

Spindle speed (rpm)	Axial cutting stability limit (mm)	
	Tool 1	Tool 2
4353	6.3	4.7
4761	3.4	2.1
5169	1.7	3.7

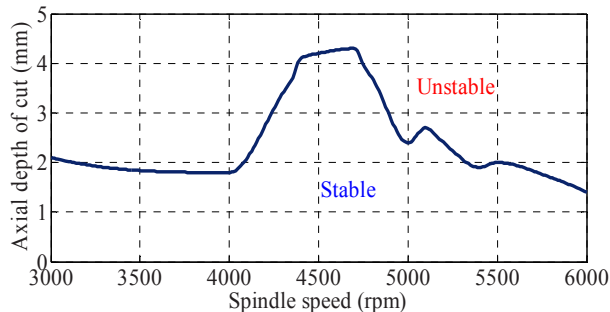


Fig. 12. Stability limits for the first tool.

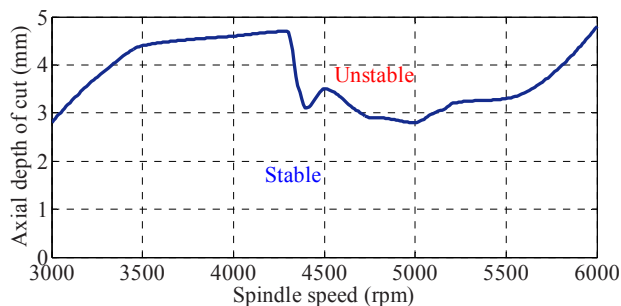


Fig. 13. Stability limits for the second tool.

7. Conclusion

A geometric model for an indexable tool with round inserts is presented. Static and dynamic cutting force models for this type of tool were developed and experimentally verified. Reasonable accuracy was shown by both models. Therefore, it can be said that the semi-empirical mechanistic evaluation of CFCs was proper. Stability limits for both tools under study were predicted. As a future work, stability limit predictions will be verified by additional cutting tests. Finally, the developed models can be used to facilitate the selection of optimum cutting parameters for different configurations of an indexable tool with round inserts of any material type, reducing time and costs of cutting trials.

Acknowledgements

This research was supported by the Advanced Manufacturing Research Centre. Assistance of AMRC staff, especially of Kareema S. Baig and Malik Bensbai in the experimental part is greatly appreciated.

References

- [1] Altintas Y., Budak E., 1995 Analytical Prediction of Stability Lobes in Milling. CIRP Annals - Manufacturing Technology, 44:357-362.
- [2] Fu H.J., Devor R. E., Kappor S.G. 1, 1984, A Mechanistic Model for the Prediction of the Force System in Face Milling Operations, ASME Journal of Engineering for Industry, 106:81-85.
- [3] Engin S. and Altintas Y. 2001, Mechanics and Dynamics of General Milling Cutters. Part II: Inserted Cutters, International Journal of Machine Tools and Manufacture, 41: 2213-2231.
- [4] Altintas Y., Kilic Z., Kaymakci M. 2012, Unified Cutting Force Model for Turning, Boring, Drilling and Milling Operations, International Journal of Machine Tools and Manufacture, 54-55: 34-45.
- [5] Kim S.J., Lee H.-U., Cho D. 12-13, 2006, Feed Rate Scheduling for Indexable End Milling Process Based on an Improved Cutting Force Model, International Journal of Machine Tools and Manufacture, Vol. 46:1589-1597.
- [6] Liu Z. Q., Cao. C. M., Du J., Shi Z. Y. 2012, Effect of Cutting Speed on Surface Integrity in High Speed Machining Nickel-Based Superalloy Inconel 718. 697, 208-212.
- [7] Yusuf Altintas, 2000, Manufacturing Automation Metal Cutting Mechanics, Machine Tool Vibrations, and CNC Design, Cambridge University Press.
- [8] Gradisek K., Kalveram J., Weinert M. 2013, Mechanistic Identification of Specific Force Coefficients for a General End Mill. International Journal of Machine Tools & Manufacture, 44:401-414.
- [9] Ozturk E, Taylor C. M., Turner S. and Devey M, 2011, Modelling and Development of a High Performance Milling Process with Monolithic Cutting Tools, AIP Conf. 1353:663-668.
- [10] Schmitz T. L., Smith K S., 2008, Machining Dynamics: Frequency Response to Improved Productivity. Springer.